

Optimization of MR Acquisition for Brain Irradiation

Veit Mengling, M.Sc.¹; Christoph Bert, Ph.D.¹; Rosalind Perrin, Ph.D.¹; Siti Masitho, M.Sc.¹; Johanna Grigo¹; Thomas Weissmann, M.D.¹; Sina Mansoorian, M.D.¹; Hadi Siavooshhaghghi¹; Rolf Janka, M.D.²; Sylvain Doussin, Ph.D.³; Melanie Habatsch³; Rainer Fietkau, M.D.¹; Florian Putz, M.D.¹

¹Department of Radiation Oncology, University Hospital Erlangen, Friedrich-Alexander-University Erlangen-Nuremberg, Erlangen, Germany

²Institute of Radiology, University Hospital Erlangen, Friedrich-Alexander-University Erlangen-Nuremberg, Erlangen, Germany

³Siemens Healthineers, Erlangen, Germany

This article has been adapted from the original publication [23] under Creative Commons Attribution 4.0 International License <http://creativecommons.org/licenses/by/4.0/>.

Abstract

MRI is a crucial factor for accurate treatment planning for brain irradiation. Currently, most sites use MR images acquired by radiologists. Although these images provide excellent diagnostic information, they often lack the level of geometric precision required for treatments like stereotactic radiosurgery. In this work, we summarize and discuss our advances in optimizing MR image acquisition for treatment planning of brain irradiation.

Introduction

MR images acquired for diagnostic uses aim to detect previously unknown pathologies and provide information on differential diagnosis. On the other hand, MR images used for radiotherapy purposes require a geometrically accurate and clear depiction of the tumor and organs at risk (OAR) in three-dimensional space for accurate delineation. Due to physical limitations, both requirements can only be

met at the same time with excessive measurement times, which often cannot be realized in clinical workflows. Therefore, a tradeoff between image quality and geometric precision has to be found.

Positioning of the patient is also different in diagnostic radiology and during radiotherapy. One of the main reasons is that most positioning and immobilization aids used in radiotherapy are either not MR-compatible, or do not fit inside the bore of the MR scanner. The different position of the patient during MRI and planning-CT acquisition can lead to registration problems because of different anatomies shown in the images.

In this article, we present our advances in the optimization of MR imaging for brain radiotherapy. For that, MR acquisition protocols optimized for radiotherapy purposes, and a novel coil setup for image acquisition in treatment position will be introduced and discussed.



1 Setup for MR imaging in treatment position for brain tumor patients. (1A) shows the commercially available setup with two 4-channel Flex coils, (1B) shows our novel proposed setup with two 18-channel UltraFlex coils. In both setups, the coils are wrapped around the head of the patient, closing under the tabletop and above the nose of the patient. The most notable differences are the fixation and connection of the coils. The mask holder is a self-built wooden replica of the metallic one used during irradiation.

Material and methods

Setup

A 1.5T MAGNETOM Sola with the MAGNETOM RT Pro Edition (Siemens Healthcare, Erlangen, Germany) was installed in December 2018 and has been used for radiotherapy planning since March 2019. It has a 70 cm bore size, second-order active shimming, and a maximal field of view (FOV) of $50 \times 50 \times 50 \text{ cm}^3$. The maximum gradient amplitude is 45 mT/m and the maximum slew rate is 200 T/m/s.

It is equipped with the INSIGHT system (Qfix, Avondale, PA, USA) including an MR-compatible flat tabletop with indexing capability. The flat tabletop allows imaging with the spine coil. The system also comes with coil holders (Qfix) for the 18-channel body coil and two 4-channel flexible coils (Siemens Healthineers) that can be used to form a head coil. The body coil holder allows for reliable coil positioning without the coil touching the patient. An MR-compatible Lok-Bar (CIVCO Medical Solutions, Kalona, IA, USA) with three pins enables consistent positioning of immobilization devices.

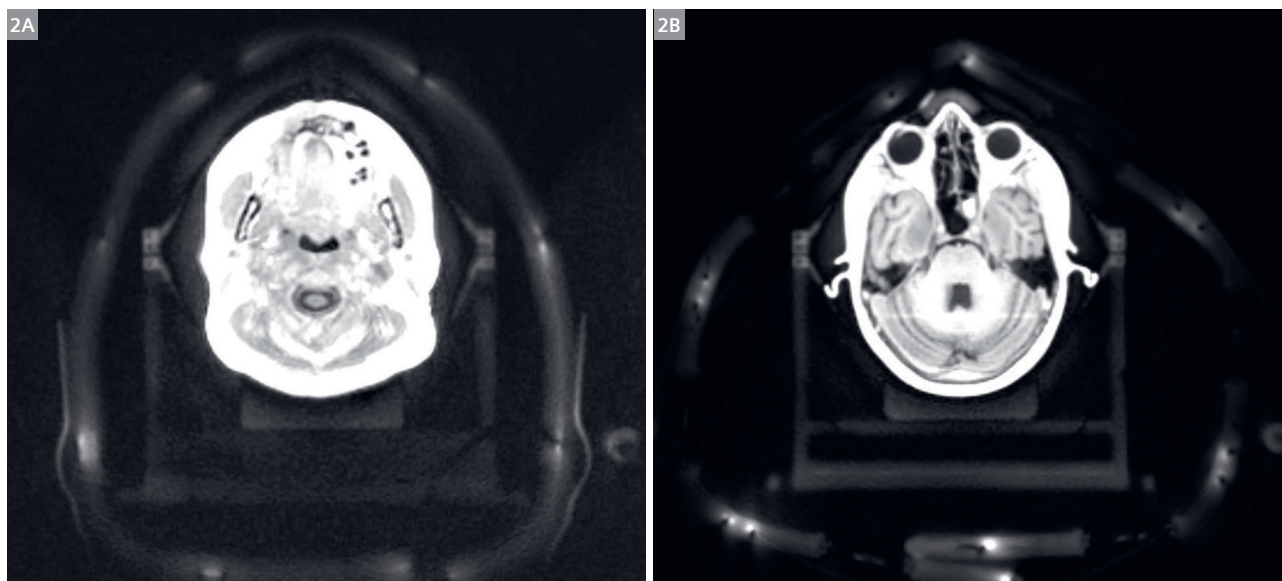
Two laser systems are available for patient positioning. Aside from the standard internal MR laser, an additional MR-compatible external laser bridge (DORADOnova MR3T, LAP of America Laser Applications, Boynton Beach, FL, USA) was installed. It consists of six sagittal, transverse, and coronal lasers, and allows patient localization, iso-center marking, and direct laser steering to set skin marks.

For head acquisitions intended to guide stereotactic radiosurgery (SRS), patients were positioned with stereo-

tactic mask immobilization (Brainlab, Munich, Germany). As the mask manufacturer did not provide MR-compatible mask holders at the time of implementation, an in-house built wooden mask holder was constructed that is compatible with the flat tabletop. Two surface-coil setups with, respectively, 8 and 36 receiving channels were investigated (see Figs. 1 and 2): 1) A commercially available setup consisting of two receiving coils (4-channel Flex Large) and the respective coil holder, and 2) our novel setup, which also consists of two receiving coils (18-channel UltraFlex Large, Siemens Healthcare) but significantly more receiving channels. The intention was to increase the signal to noise ratio (SNR) as well as image quality for target and OAR delineation, as the wooden mask holder induced an additional distance between the coils and the patient compared to the standard setup. As the UltraFlex coils are larger than the Flex coils, the coil holder could not be used in the novel setup. Reproducible positioning was instead achieved by placing cushions under the UltraFlex coils and fixing them with two Velcro straps at the top (see Fig. 1B).

Image-quality evaluation

As part of routine clinical practice, most patients received MR imaging in one of the above-described surface-coil setups in treatment position as well as in a standard diagnostic setup (Head/Neck 20-channel coil) in the same session to enable optimal diagnostic assessment as well as dedicated imaging for treatment planning. To evaluate the image quality of the two setups in treatment position, the SNR of each setup was compared with the SNR in the standard diagnostic radiology setup (Head/Neck



2 Axial view of the (2A) 4-channel Flex coil setup and the (2B) 18-channel UltraFlex coil setup. As the image quality was worse in 2A and the coils have fewer visible elements, different windowing and slice positioning was chosen for the two images.

20-channel coil). As the SNR was not homogeneous along the anterior-posterior direction, the evaluation was split into the anterior, the central, and the posterior part of the head. To calculate the SNR, the mean intensity in a circular region of interest (ROI) in white matter was divided by the standard deviation of a circular ROI in the background in the corresponding section. To ensure a homogeneous signal and that the coil profile did not affect SNR calculation, the circular ROIs were at least 0.5 cm² in the white matter and between 4 and 5 cm² in the background. The SNR was calculated on both the transversal T1w-MPRAGE sequence after contrast-agent injection and on the T2w-FLAIR (for detailed parameters see Table 1).

The suitability for contouring was assessed by three experienced radiation oncologists (FP, TW, SM). Images of the three setups (154 in total) were blinded, loaded into 3DSlicer (v. 4.10.2) [1], and presented to the physicians in randomized order. The radiation oncologists then graded each image on a scale of 1 (not suitable for contouring) to 4 (excellent suitability for contouring), based on the image quality and the distinguishability of the lesions from the surrounding tissue using a custom-made software module in randomized order. Additionally, the radiation oncologists counted the number of metastases for every data set with a similar software module in randomized order and in a blinded fashion.

	T2w-TSE-FLAIR	T2w-SPACE-Dark-Fluid	T1w-MPRAGE	T1w-SPACE	EPI with shaped excitation (ZOOMit)
Voxel size [mm x mm x mm]	0.7 x 0.7 x 5.0	0.5 x 0.5 x 1.0	1.0 x 1.0 x 1.0	0.5 x 0.5 x 1.0	0.8 x 0.8 x 3.0
Orientation	Transversal	Transversal	Transversal	Transversal	Coronal
Dimension	2D	3D	3D	3D	2D
Contrast agent	yes	yes	yes	yes	yes
Flip angle [°]	150	120 (T2 Var)	8	120 (T1 Var)	90
TR [ms]	9000	7000	2200	700	4000
TE [ms]	93	374	3.02	22 19	65
TI [ms]	2500	2050	900		
Fat-saturation	yes	yes	no	yes	yes
Bandwidth [Hz/Px]	130	751	160	399	1221

Table 1A: Detailed sequence parameters of the protocols used for head imaging.

	T2w-SPACE	Dixon	T2w-BLADE	RESOLVE ok	EPI with shaped excitation (ZOOMit)
Voxel size [mm x mm x mm]	0.9 x 0.9 x 1.0	1.6 x 1.6 x 2.0	0.6 x 0.6 x 3.0	0.9 x 0.9 x 4.8	0.8 x 0.8 x 3.0
Orientation	Transversal	Transversal	Sagittal	Transversal	Transversal
Dimension	3D	3D	2D	2D	2D
Contrast agent	no	no	no	no	no
Flip angle [°]	155	15	160	180	90
TR [ms]	1200	6.2	5820	8060	4000
TE [ms]	138	2.39/4.77	117	60/98	70
Fat-saturation	no	no	no	yes	yes
Bandwidth [Hz/Px]	651	1015	178	994	1221

Table 1B: Detailed sequence parameters of the protocols used for prostate imaging.

Significance of the qualitative grading results was tested using a Welch two-sample t-test. To compare the number of counted metastases between the diagnostic setup and the novel UltraFlex setup in treatment position, a paired t-test was used. Calculations were performed using R and SPSS v.21. The level of significance was set at $P < 0.05$.

As the positioning in a thermoplastic mask was hypothesized to enable better immobilization than the standard diagnostic setup, motion artifacts in T1w-MPRAGE images of patients who received scans both in the treatment position and in the radiologic setup were compared. If motion artifacts were clearly identifiable in either OAR or target volumes, the image was classified as motion-corrupted.

Sequence protocols

MRI sequences for radiotherapy planning should depict the three-dimensional boundaries of target volumes and organs at risk with the highest geometric accuracy and as clearly as possible. As the main emphasis of diagnostic imaging lies on the identification and characterization of diseases, dedicated sequence optimization for the purpose of RT planning is needed.

Whenever possible, isotropic 3D sequences should be used, as they reduce distortions and enable accurate multiplanar reconstructions. [2] Slice thickness should be as low as possible, with the exact value depending on site- and treatment-specific considerations and a general rule of thumb is that structures should be visualized on at least 5 slices to minimize over- or underestimation of volumes due to partial-volume effects [2, 3]. As geometric precision is affected by various mechanisms in MR imaging, specific methods should be applied to counteract these effects. To decrease the geometric distortions caused by gradient nonlinearities, vendor-provided 3D distortion correction should always be applied as a minimum [2]. As susceptibility-induced distortions can lead to errors in frequency-encoding-direction, active shimming on a per-patient basis should be used and the receiver bandwidth should be set as high as possible [2, 4, 5].

Before creating the core protocols, we formulated the following site- and disease-specific clinical objectives.

Brain metastases

MRI sequences in brain metastases should be able to depict the three-dimensional contrast-enhancing tumor volumes as accurately as possible without gaps. As brain metastases frequently measure 5 mm or less in diameter, resolution should be high in every image dimension to minimize partial-volume effects. Contrast ratio between lesions and surrounding brain parenchyma should be optimized to allow accurate delineation and minimize interobserver variability.

Gliomas

Similar considerations were applied for gliomas. However, emphasis on the most accurate depiction of the contrast enhancement was lower than in metastases, as the volume of contrast enhancement – if present – and clinically employed margins usually are much larger in gliomas than in metastases. In addition, the volume of contrast enhancement in malignant gliomas only represents a fraction of all tumor cells, with glioma cells extending far beyond the boundaries of the contrast enhancing area. Therefore, more emphasis was put on accurate depiction of the surrounding T2w-FLAIR hyperintensity, which may represent non-enhancing tumor or microscopic disease extension. T2w-FLAIR hyperintensity should be depicted in high-resolution and continuously without slice gaps.

As contrast-enhancing tumor and post-therapeutic changes are frequently difficult to differentiate in recurrent gliomas, additional information for contouring should be provided by a high resolution diffusion-weighted sequence.

Results

Patients

The data in this study results from patients who received an MRI scan within the first year after installation of the scanner. A total of 89 patients were included, with 19 patients receiving multiple scans. As the images were taken as part of standard clinical care, not all patients received imaging in a mask setup and the radiology setup. Additionally, not all patients received a T2w-FLAIR, as it was not needed for therapy in every case. In total, 11 T1w-MPRAGE images were acquired in the Flex coil setup, 83 in the UltraFlex coil setup, and 60 in the radiology setup. 10 T2w-FLAIR images were acquired in the Flex coil setup,

	Head coil	Flex coil	UltraFlex coil
	T1w MPRAGE		
Anterior	102±22	84±8	163±28
Central	95±20	68±6	104±23
Posterior	119±23	56±7	78±14
	T2w FLAIR		
Anterior	91±11	62±7	107±13
Central	87±9	58±7	86±11
Posterior	98±16	51±10	64±8

Table 2: Mean SNR (± standard deviation) of the radiology setup (Head coil, n = 60), the vendor-provided setup (Flex coil, n = 83) and our novel setup (UltraFlex coil, n = 11).

65 in the UltraFlex coil setup, and 37 in the radiology setup. For more details on the patients, see Table 2.

Motion artifacts

Of the 60 patients imaged in the diagnostic setup, eight showed severe motion artifacts in the radiology setup that were visible in treatment relevant regions. In contrast, no relevant motion artifacts could be detected in both the novel setup and the commercially available setup, in which patients were imaged in treatment position with mask immobilization.

SNR

The mean SNR for the three setups is shown in Table 2. In the novel setup, it decreased from anterior to central and from central to posterior for both investigated sequences. The SNR in the commercially available setup also decreased from anterior to central and from central to posterior for both sequences. The anterior and central SNR in the radiology setup showed no significant difference, while the SNR in the posterior part of the head was higher than in the anterior and the central part of the head for both sequences.

The SNR of the novel setup for both sequences was higher than the SNR in the radiology setup anteriorly, but lower posteriorly. Centrally, it was higher than in the radiology setup for the T1w-MPRAGE. For the T2w-FLAIR, no significant difference was found centrally. In contrast, the SNR of the commercially available setup was lower

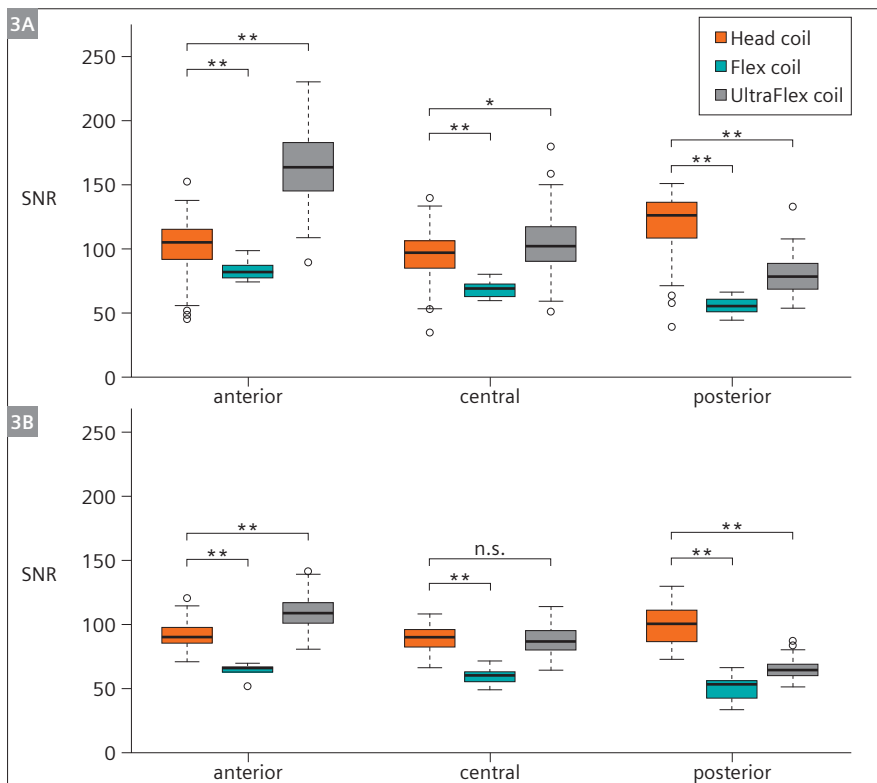
anteriorly, centrally, and posteriorly. For more details of the distribution, see Figure 3.

Blinded expert-based assessment of image quality

The qualitative grading of the image quality showed a median score of 2 (“suitable for contouring”) for all three setups in a randomized and blinded assessment. No significant difference could be found between the setups ($0.1 < P < 0.4$). Furthermore, in a randomized and blinded comparison, there was no significant difference in the number of identified brain metastases between the diagnostic setup and the novel high-channel UltraFlex setup (mean number of identified brain metastases 3.4 vs. 3.2, $P = 0.369$). Figure 4 shows images of a patient who received imaging in all three setups.

Sequences used

According to the requirements and objectives defined in the previous section, the following core protocols were established. Detailed sequence parameters can be found in Table 1. Brain measurements are mostly taken with the novel high-channel UltraFlex setup. All sequences use active shimming to reduce patient-induced distortions as well as 3D distortion correction to reduce system-induced distortions. To further reduce the effect of patient-induced distortions, the bandwidth was set to the highest value possible while keeping acceptable SNR and acquisition time.



3 Boxplot of the SNR of the different coil setups in the anterior, central, and posterior part of the head measured on (3A) the contrast enhanced T1w-MPRAGE and (3B) the T2w-FLAIR. * indicates a significance level of $P < 0.05$, ** indicates a significance level of $P < 0.01$.

Brain metastases

Gadolinium-based contrast agent is injected immediately after completing the localizer. To ensure sufficient contrast uptake, a transversal T2w-FLAIR is acquired. After that, a high-resolution $0.5 \times 0.5 \times 1.0 \text{ mm}^3$ transversal T1w-SPACE is acquired. The total acquisition time was 14:29 min.

Gliomas

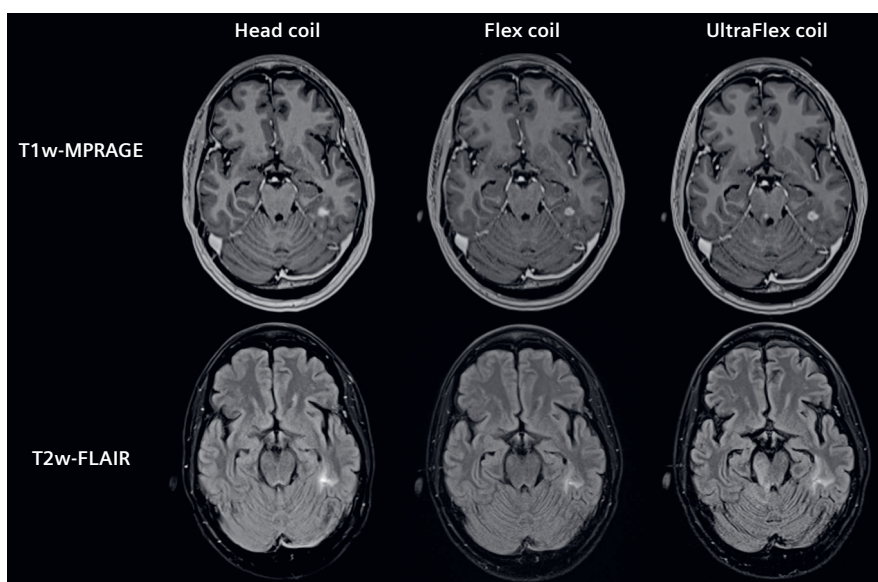
The core protocol also starts with contrast agent injection right after completing the localizer. A $0.5 \times 0.5 \times 1 \text{ mm}^3$ transversal T2w Dark Fluid is acquired next, followed by a $1.0 \times 1.0 \times 1.0 \text{ mm}^3$ isotropic transversal T1w-MPRAGE. For the diffusion sequence, an EPI-ZOOMit with $0.8 \times 0.8 \times 3.0 \text{ mm}^3$ resolution was chosen to enable a high-resolution assessment of diffusion-weighted image changes. The total acquisition time was 26:42 min.

Discussion

Both tested coil setups in treatment position are suited for use in treatment planning of brain irradiation. Compared to the diagnostic gold standard, the mean SNR of the novel setup on both the T1w-MPRAGE and the T2w-FLAIR was better in the anterior part of the head, slightly better in the central part of the head (no significant difference for the T2w-FLAIR), and worse in the posterior part of the head. The variance of the SNR in anterior-posterior direction of our novel setup was higher than in the radiology setup. The SNR in the novel setup was significantly higher in all parts of the head compared to the commercially available Flex coil setup. The anterior-posterior distribution was comparable. This can be explained by the distance of the receive coils to the imaged volume. In the radiology setup, the SNR is highest in the posterior part of the head, where the head lies directly over the receive element. The anteri-

or and the central part of the head are further away from the coil, resulting in lower SNR. The same reasoning leads to the non-uniform distribution for the UltraFlex and Flex coil setup. While the anterior part of the head is in direct contact with the coil, the head rest and flat tabletop overlay led to a distance of about 9 cm between the receive coils and the back of the head. The lower SNR in the posterior part of the head might be improved by adding a small coil in the back of the mask holder. While the combination of coils would need to be tested, a superior SNR with our novel setup may likely be achievable in all parts of the head compared to the radiology set up in the Head/Neck 20 coil. However, this would mean that mask systems without additional elevation on top of the tabletop would show a more homogeneous SNR.

The median qualitative grading of the image quality showed no difference between the three tested setups. This means that the novel setup is not inferior to the diagnostic radiology gold standard, while allowing imaging in treatment position. However, this also means that it is not significantly better than the setup with the smaller Flex coils. One possible explanation is the small sample size ($n = 11$) for the Flex coil setup compared to the novel UltraFlex setup ($n = 83$). Another explanation is that the image quality of the two flexible coil setups highly depends on the inspected part of the head. This results in lower scores for posterior lesions compared to anterior lesions. The mean SNR in the posterior part of the head is also more similar between the setups than in the anterior part of the head, which could explain the similar ratings. Most images rated in this work had their lesions in the posterior part of the head. As no significant difference in the number of detected metastases was found between the setups, the SNR is still high enough to reliably detect the lesions.



4 Images of a patient in all three investigated setups. The top row shows images of the contrast-enhanced T1w-MPRAGE, while the bottom row shows images of the T2w-FLAIR. The images in the left and middle column were acquired on the same day, the images in the right column were acquired 77 days later. The contrast-enhancing lesion and the FLAIR hyperintensity can be seen clearly in all three setups. While the head coil shows relatively homogeneous SNR, the noise in both mask setups increases significantly in anterior-posterior direction.

All coil setups produced images that were suitable for contouring. Our novel setup, however, combines the advantages of the commercially available setup and the standard radiology setup as it allows for high-quality imaging in RT treatment position. Additionally, positioning in a thermoplastic mask leads to reduced motion artifacts. In our case, no motion artifacts were observed in the mask setups, while some groups report movement to be less than 1.5 mm [6].

The current state of the art coil setup for RT treatment planning consists mainly of flexible surface loop coils with a low number of channels [7–9]. They have been reported to have a significantly worse SNR than diagnostic coils [8]. In comparison, the SNR of our novel setup is significantly higher both anteriorly and centrally, and lower posteriorly compared to the diagnostic coil setup, while having the same suitability for contouring. Therefore, our novel setup can be seen as an improvement over the state-of-the-art setup. The setup is also less prone to setup errors, as the coils only fit under the tabletop in a specific way. This reduces the influence of technician dependent coil positioning, which can be a problem for surface flexible loop coils [10].

Another advantage of our setup is the possibility to use almost all mask immobilization systems, which usually don't fit into the diagnostic head coil. For example, our setup can be extended for head-neck examinations by adding the Body Long coil with the body coil holder to cover the neck area. Different mask systems will most likely need adapters to attach the masks to the tabletop. If not commercially available, these can be built relatively easily, as demonstrated by our in-house built wooden mask holder.

The protocols we developed are in accordance with a recently published consensus paper on MRI simulation [2]. Active shimming, 3D acquisition, and distortion correction were applied whenever possible.

In our brain metastases protocol, we acquire two high-resolution, contrast-enhanced T1w images. Currently, the T1w-MPRAGE is still the most widely used sequence for imaging of brain tumors [11, 12]. However, there is growing evidence that the T1w-SPACE could be superior to the T1w-MPRAGE for intracranial target volume delineation [11, 13, 14]. Therefore, we performed both sequences for brain metastases. While we could see the target volumes better on the T1w-SPACE in most cases, the T1w-MPRAGE still sometimes provided better contrast. The generally superior conspicuity of lesions in the T1w-SPACE in our experience can be largely attributed to the lower contrast between white matter and gray matter. Often it is beneficial to acquire diffusion-weighted images of the whole brain to aid tumor visualization, especially if treatment-related contrast enhancement is present following surgery or radiation. This can be achieved by an EPI-sequence. For a limited field-of-view an additional EPI-ZOOMit can be useful, as it provides better resolution.

The glioma protocol features a high-resolution T2w Dark Fluid that allows high-resolution imaging of the T2w-FLAIR hyperintensity. As this sequence is significantly longer than a standard T2w-FLAIR, we decided to only include one contrast-enhanced T1w sequence. Ideally the T1w-SPACE should be chosen because it has been shown to provide favorable conspicuity and contrast ratio in comparison to the T1w-MPRAGE in patients with gliomas [11]. However, since mostly the acquisition time slot is limited, we chose the T1w-MPRAGE. The EPI-ZOOMit allows high-resolution diffusion imaging of the investigated volume.

Our experiences in fine-tuning the protocols from the starting point of the diagnostic sequence settings showed that standard parameters like TE, TR, or TI are almost always adjusted optimally for radiotherapy uses, too. The voxel resolution in diagnostic sequences, however, can be slightly non-isotropic, which is undesirable for RT purposes. Additional, standard diagnostic sequences often only employ 2D-distortion correction, if any, which is potentially a relic from times when 3D-distortion correction was relatively computationally demanding. Although most sequences come with active shimming enabled by default, the shimming type should be checked for every sequence. As we only changed parameters that could diminish the quality of the imaging and the sequences, we optimized for precision based on diagnostic sequences, the resulting precision should be at least equal to that of the well-established diagnostic sequences. Protocol time is also a major factor in protocol development. Therefore, it is important to get a feeling for which acceleration techniques yield the optimal results for each sequence type. While most sequences in our protocols are accelerated by parallel imaging techniques such as GRAPPA [15], we also tested compressed sensing. The success of this technique highly depends on the sequence it is used on. For the T2w-SPACE used in the prostate protocol, an acceleration factor of 8 with compressed sensing produced high quality images with significantly reduced acquisition time. Compressed sensing resulted in blurred contours of the metastases when applied to the T1w-SPACE in our brain protocols with large acceleration factors and automatic noise reduction. However, using a low compressed sensing acceleration factor of 2.5 with subtle manual noise reduction provided good image quality and reduced scan duration, thereby further improving our RT planning protocol.

The setup presented in this work is optimally suited for an MR-only workflow, where imaging has to be performed in treatment position. The diagnostic image quality that can be achieved with our setup, as well as the possibility to generate head pseudo-CTs based on these images for dose calculation [16–19], make it an optimal choice for MR-only workflows in head treatments. Head-Neck MR-only workflows may be realized by adding the body coil to our setup to produce high quality head-neck images. A prostate

MR-only workflow can also be realized by calculating a pseudo-CT based on the MRI images. This leads to a more efficient workflow, reducing the number of examinations for a patient and therefore avoiding additional ionizing radiation [20]. Vendor-provided automated algorithms to calculate pseudo-CTs are available on our MR scanner that enable MR-only workflows without the need for additional planning CTs and image coregistration [21]. We are currently evaluating the dosimetric accuracy of the pseudo-CTs; while in our experience problems may arise in post-operative situations, other groups have found excellent agreement for focal brain VMAT radiotherapy with $D_{95\%}$ differences of 0.0% [22].

Conclusion

In this work, we presented a novel setup for brain imaging in treatment position with mask immobilization. We showed that with two UltraFlex coils diagnostic image quality in treatment position with mask immobilization can be achieved. By building a mask holder that fits the specific immobilization system, our coil setup could be used for a range of mask systems. We also shared our initial experiences with implementing dedicated RT-planning protocols and presented the core protocols we employed for radiotherapy treatment planning. For the interested reader, a more detailed discussion of the results can be found in our original publication [23].

References

- Kikinis, R., S.D. Pieper, and K.G. Vosburgh, 3D Slicer: A Platform for Subject-Specific Image Analysis, Visualization, and Clinical Support, in *Intraoperative Imaging and Image-Guided Therapy*, F.A. Jolesz, Editor. 2014, Springer New York: New York, NY. p. 277-289.
- Paulson, E.S., et al., Consensus opinion on MRI simulation for external beam radiation treatment planning. *Radiother Oncol*, 2016. 121(2): p. 187-192.
- Snell, J.W., et al., Assessment of imaging studies used with radiosurgery: a volumetric algorithm and an estimation of its error. Technical note. *J Neurosurg*, 2006. 104(1): p. 157-62.
- Emmerich, J., et al., Technical Note: On the size of susceptibility-induced MR image distortions in prostate and cervix in the context of MR-guided radiation therapy. *Med Phys*, 2018. 45(4): p. 1586-1593.
- Walker, A., et al., MRI distortion: considerations for MRI based radiotherapy treatment planning. *Australas Phys Eng Sci Med*, 2014. 37(1): p. 103-13.
- Mandija, S., et al., Brain and Head-and-Neck MRI in Immobilization Mask: A Practical Solution for MR-Only Radiotherapy. *Front Oncol*, 2019. 9(647): p. 647.
- Liney, G.P., et al., Commissioning of a new wide-bore MRI scanner for radiotherapy planning of head and neck cancer. *Br J Radiol*, 2013. 86(1027): p. 20130150.
- Wong, O.L., et al., Image quality assessment of a 1.5T dedicated magnetic resonance-simulator for radiotherapy with a flexible radio frequency coil setting using the standard American College of Radiology magnetic resonance imaging phantom test. *Quant Imaging Med Surg*, 2017. 7(2): p. 205-214.
- Winter, R.M., et al., Assessment of image quality of a radiotherapy-specific hardware solution for PET/MRI in head and neck cancer patients. *Radiother Oncol*, 2018. 128(3): p. 485-491.
- Ruytenberg, T., et al., Improvements in High Resolution Laryngeal Magnetic Resonance Imaging for Preoperative Transoral Laser Microsurgery and Radiotherapy Considerations in Early Lesions. *Front Oncol*, 2018. 8: p. 216.
- Danieli, L., et al., Brain Tumor-Enhancement Visualization and Morphometric Assessment: A Comparison of MPRAGE, SPACE, and VIBE MRI Techniques. *AJNR Am J Neuroradiol*, 2019. 40(7): p. 1140-1148.
- Ellingson, B.M., et al., Consensus recommendations for a standardized Brain Tumor Imaging Protocol in clinical trials. *Neuro Oncol*, 2015. 17(9): p. 1188-98.
- Reichert, M., et al., Contrast-enhanced 3-dimensional SPACE versus MP-RAGE for the detection of brain metastases: considerations with a 32-channel head coil. *Invest Radiol*, 2013. 48(1): p. 55-60.
- Komada, T., et al., Contrast-enhanced MR imaging of metastatic brain tumor at 3 tesla: utility of T(1)-weighted SPACE compared with 2D spin echo and 3D gradient echo sequence. *Magn Reson Med Sci*, 2008. 7(1): p. 13-21.
- Griswold, M.A., et al., Generalized autocalibrating partially parallel acquisitions (GRAPPA). *Magn Reson Med*, 2002. 47(6): p. 1202-10.
- Maspero, M., et al., Dose evaluation of fast synthetic-CT generation using a generative adversarial network for general pelvis MR-only radiotherapy. *Phys Med Biol*, 2018. 63(18): p. 185001.
- Dinkla, A.M., et al., MR-Only Brain Radiation Therapy: Dosimetric Evaluation of Synthetic CTs Generated by a Dilated Convolutional Neural Network. *Int J Radiat Oncol Biol Phys*, 2018. 102(4): p. 801-812.
- Dowling, J.A., et al., Automatic Substitute Computed Tomography Generation and Contouring for Magnetic Resonance Imaging (MRI)-Alone External Beam Radiation Therapy From Standard MRI Sequences. *Int J Radiat Oncol Biol Phys*, 2015. 93(5): p. 1144-53.
- Koivula, L., et al., Intensity-based dual model method for generation of synthetic CT images from standard T2-weighted MR images - Generalized technique for four different MR scanners. *Radiother Oncol*, 2017. 125(3): p. 411-419.
- Hanvey, S., et al., The influence of MRI scan position on patients with oropharyngeal cancer undergoing radical radiotherapy. *Radiat Oncol*, 2013. 8: p. 129.
- Hsu, S.H., et al., Investigation of a method for generating synthetic CT models from MRI scans of the head and neck for radiation therapy. *Phys Med Biol*, 2013. 58(23): p. 8419-35.
- Paradis, E., et al., Assessing the Dosimetric Accuracy of Magnetic Resonance-Generated Synthetic CT Images for Focal Brain VMAT Radiation Therapy. *Int J Radiat Oncol Biol Phys*, 2015. 93(5): p. 1154-61.
- Mengling, V., et al., Implementation of a dedicated 1.5T MR scanner for radiotherapy treatment planning featuring a novel high-channel coil setup for brain imaging in treatment position. *Strahlenther Onkol* 197, 246 -256 (2021). <https://doi.org/10.1007/s00066-020-01703-y>

Contact

Professor Christoph Bert, Ph.D.
 Department of Radiation Oncology
 Friedrich-Alexander-University Erlangen-Nuremberg
 Universitaetsstraße 27
 91054 Erlangen
 Germany
 Phone: +49 (0)9131 85-44213
 Christoph.bert@uk-erlangen.de